Search for WIMP Inelastic Scattering Off Xenon Nuclei With XENON100 Data

(The XENON100 Collaboration)

(Dated: January 19, 2017)

Some nice abstract here.....

I. INTRODUCTION

Astrophysical and cosmological evidence indicates that the dominant mass fraction of our Universe consists of some yet unknown form of dark, or invisible matter. The dark matter could be made of new, stable or long-lived and yet undiscovered particles. Well-motivated theoretical models going beyond the Standard Model of particle physics predict the existence of Weakly Interacting Massive Particles (WIMPs), which are natural candidates for dark matter. This hypothesis is currently being tested by several direct and indirect detection experiments, as well as at the LHC [1, 2].

Most direct detection searches focus on elastic scattering of galactic dark matter particles off nuclei, where the keV-scale nuclear recoil energy is to be detected [3–5]. In this work, the alternative process of inelastic scattering is explored, where a WIMP-nucleus scattering induces a transition to a low-lying excited nuclear state. The experimental signature is a nuclear recoil detected together with the prompt de-excitation photon [6].

We consider the ^{129}Xe isotope, which has an abundance of 26.4% in natural xenon, and a lowest-lying $3/2^+$ state at 36.6 keV above the $1/2^+$ gound state. The electromnagnetic nuclear decay has a half-life of 0.97 s. The signatures of inelastic scattering in xenon have been studied in detail in [7]. It was found that this channel is complementary to spin-dependent, elastic scattering, dominating the integrated rates above $\simeq 10$ keV energy depositions. In addition, in case of a positive signal, the observation of inelastic scattering would provide a clear indication of the spin-dependent nature of the fundamental interaction.

Our paper is structures as follows. In Section II we briefly describe the XENON100 detector and the employed data set in this analysis. In Section III we detail the data analysis method, including the simulation of the expected signal and the background model. We conclude in Section IV with our results and new constraints on inelastic WIMP-nucleus scatters.

II. THE XENON100 DETECTOR

The XENON100 experiment operates a dual-phase (liquid and gas) xenon time projection chamber (TPC) at the Laboratori Nazionali del Gran Sasso (LNGS) in Italy. It contains 161 kg of xenon in total, with 62 kg in the active region of the TPC. These are monitored by 242 1-inch square, low-radioactivity, UV-sensitive photomultiplier tubes (PMTs) arranged in two arrays, one in the liquid and one in the gas. The PMTs detect the prompt scintillation (S1) and the delayed, proportional scintillation signal (S2) created by a particle interacting in the active TPC region. The S2-signal is generated due to ionisation electrons, drifted in an electric field of 530 V/cm and extracted into the gas phase by a stronger field of ~ 12 kV/cm, where the proportional scintillation, or electroluminiscence, is produced. These photons carry the (x, y) information of the interaction site, while the $z-$information comes from the drift time measurement. The TPC thus yields a three-dimensional event localisation, with an (x, y) resolution of <3 mm $(1\,\sigma)$, and a z resolution of <0.3 mm $(1\,\sigma)$, enabling to reject the majority of background events via fiducial volume cuts [8]. The ratio S2/S1 provides the basis for distinguishing between nuclear recoils (NRs), as induced by fast neutrons and expected from elastic WIMP-nucleus scatters, and electronic recoils (ERs) produced by β and γ-rays.

XENON100 has acquired science data between 2008-2015, and has set competitive constraints on spin-independent [9, 10] and spin-dependent [10, 11] elastic WIMP-nucleus scatters, on solar axions and galactic ALPs [12], as well as on leptophilic dark matter models [13–15].

Here we explore a potential new signature in the XENON100 detector, caused by spin-dependent, inelastic WIMP-^{129}Xe scatters. The expected inelastic scattering signature is a combination of an ER and a NR, due to the short lifetime of the excited nuclear state and the short mean free path of $\sim$0.15 mm of the 39.6 keV de-excitation photon.

III. DATA ANALYSIS

This analysis is performed using XENON100 Run-II science data, which corresponds to a data set with an exposure of 224.6 live days. The detector response to ERs has been characterised with ^{60}Co and ^{232}Th calibration sources, while the response to NRs was calibrated with an ^{241}AmBe (α, n)-source. This fast neutron source gives rise to elastic and inelastic neutron-nucleus scatters, and can thus be employed to define the expected signal region for inelastic WIMP-nucleus scatters.

A. Signal Correction

A particle interaction in the liquid xenon produces an S1 and a correlated S2 signal with a certain number of photoelectrons (PE) observed by the PMTs. The non-uniform scintillation light collection by the PMT arrays, due to solid angle effects, Rayleigh scattering length, reflectivity, transmission of the electrodes, etc, lead to a position-dependent S1 signal. The warping of the top meshes (inducing a variation in the width of the gas gap between the anode and the liquid-gas interface), the absorption of electrons by residual impurities as they drift towards the gas region, as well as solid angle effects lead to a position-dependent S2 signal. These signals are thus corrected in 3 dimensions, using various calibration data, as detailed in [8, 16], with the corrected quantities denoted as cS1 and cS2, and defined in [16]. The trigger efficiency in thus run was 100% for S2>300 PE.

B. Signal Region and Event Selection

As explained in Section I, the inelastic scattering of a WIMP with a ^{129}Xe nucleus produces an energy deposit via a NR with subsequent emission of a 39.6 keV de-excitation photon. The largest fraction of the energy released in the event is via an ER, due to the emitted photon which loses its energy in the LXe. This represents an unusual signature compared to the one expected from an elastic scatter, and brings the signal region to overlap with the ER background region. The selected region of interest (ROI) for this analysis surrounds the 39.6 keV xenon line in the cS1-cS2 plane and is further divided into sub-regions, as shown in Figures 1 and 2.

Apart from the condition to occur in the defined region of interest in the cS2-cS1-plane, valid events are required to fulfil several selection criteria, which can be summarised as follows: data quality cuts, energy selection and S2 threshold cut, veto cut for events with energy release in the detectors active LXe shield, selection of single scatter events and of a predefined fiducial volume.

This analysis follows the selection criteria described in detail in [16] for Run-II, with only a few exceptions reported in what follows. The cut on the S2 signal width as a function of drift time (where the maximal drift time is 176 μs and the width values range from $\sim$1-2 μs) has been optimised on a sample of events selected from the 39.6 keV line and set to a 95% acceptance on these. Events are required to be single-scatters by applying a threshold cut on the size of the second largest S2 peak. For this analysis, the threshold has been optimised to 160 PE and set constant as function of S2 signal size. Finally, the chosen fiducial volume corresponds to 34 kg of liquid xenon.

C. Signal Simulation

The detector response to inelastic WIMP-^{129}Xe interactions was simulated using an empirical signal model. The total deposited energy is divided into two independent contributions: one coming from the 39.6 keV de-excitation photon and the other from the simultaneous nuclear recoil of the xenon atom. The detected light (S1) and charge (S2) signals are simulated separately for each of the two contributions and then added together. This is due to the fact that the light and charge yields depend on the type of interaction (ER vs. NR), and on the deposited energy.

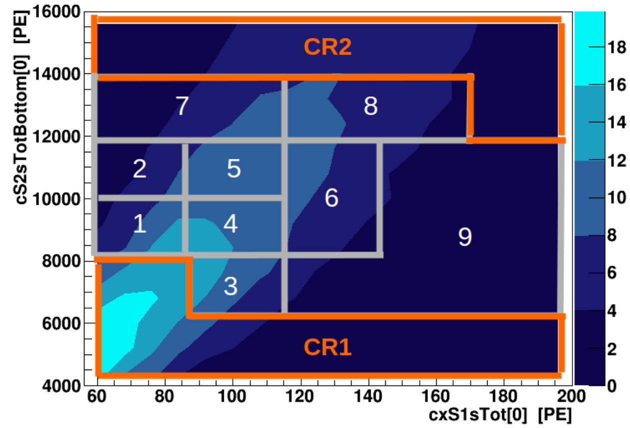

FIG. 1. Signal (1-9) and control (CR1 and CR2) regions for the inelastic WIMP-^{129}Xe interaction in the cS2 versus cS1 plane. I think we must explains the shape of these regions.

The distribution of an ER induced by the de-excitation photon in the cS1-cS2 plane is simulated assuming a two dimensional normal probability distribution function (pdf), $f(cS1, cS2)$, described (apart from a constant normalisation factor) by the following equation:

$$f(cS1, cS2) = \exp\Big\{ -\frac{1}{2(1-\rho^2)}\Big[\frac{(cS1-\mu_{cS1})^2}{\sigma_{cs1}^2} + \frac{(cS2-\mu_{cS2})^2}{\sigma_{cs2}^2} - \frac{2\rho\cdot(cS1-\mu_{cs1})(cS2-\mu_{cs2})}{\sigma_{cs1}\sigma_{cs2}}\Big]\Big\} \quad (1)$$

where μ_{cS1} and μ_{cS2} represent the average observed cS1 and cS2 signals given a 39.6 keV ER, σ_{cs1} and σ_{cs2} are the standard deviation in cS1 and cS2 respectively, while ρ stands for the correlation between the cS1 and cS2 signals. The detector-related light yield L_y at 39.6 keV, necessary to evaluate the average number of prompt photons detected (μ_{cS1}), is obtained from the NEST model [17–19] fit to data collected with several γ-lines. The average light yield at 39.6 keV is 2.7 PE/keV.

The same model is used to predict the charge yield at 39.6 keV, which is afterwards scaled according to the detector's secondary scintillation gain Y. The latter is determined from detector's response to single electrons [20]. The energy resolution at 39.6 keV in cS1 and cS2 has been measured to be 15.8% and 14.7%, respectively, and is used to extract the standard deviations σ_{cs1}, σ_{cs2}. The correlation parameter is assumed to be independent of energy (at least in the considered narrow energy range) and measured using the 164 keV line from the decay of the ^{131m}Xe isomer ($T_{1/2}$=11.8 d) produced during the ^{124}AmBe run. This γ-line is chosen because it allows to disentangle efficiently the contribution from the nuclear recoil. The measured correlation coefficient is $\rho = -0.45 \pm 0.10$.

The cS1 and cS2 distributions from the NR contribution are predicted starting from the expected nuclear recoil energy spectrum of WIMP inelastic interactions [7]. The average cS1 and cS2 are given by equations 2 and 3 respectively, where $\mathcal{L}_{eff}$ is the liquid xenon relative scintillation efficiency for NRs, while $S_{ee} = 0.58$ and $S_{nr} = 0.95$ describe the scintillation quenching of ER and NRs, respectively, due to the electric field [21]. The parameterisation and uncertainties of $\mathcal{L}_{eff}$ as a function of nuclear recoil energy E_{nr} are based on existing direct measurements [22]. The light yield for 122 keV ERs is taken from the same NEST model fit as described above. For cS2, the parameterisation of $Q_Y(E_{nr})$ is taken from [23]. Finally, all detector related resolution effects are introduced following the prescriptions described in [16].

$$cS1_{nr} = E_{nr}\,\mathcal{L}_{eff}(E_{nr})\,L_y\,\frac{S_{nr}}{S_{ee}} \quad (2)$$

$$cS2_{nr} = E_{nr}\,Q_Y(E_{nr})\,Y \quad (3)$$

The pdf of the ER and NR contributions are then convoluted together to obtain the overall pdf of the expected signal. A 2D (cS1 versus cS2) acceptance map is applied to the signal pdf to reproduce data selection effects. Acceptances are computed separately for each selection criteria using the ^{124}AmBe calibration sample. Other selections such as the liquid xenon veto cut, and the single-scatter interaction represent an exception and a dedicated computation has been performed in these cases. The combined acceptance of all selection criteria in the region of interest averages to $\sim(0.80 \pm 0.05)$. Figure 1 shows an example of fully simulated signal model for a WIMP mass of 100 GeV/c^2.

The signal simulation procedure has been validated by reproducing the 39.6 keV xenon line from interactions due to neutrons from the ^{124}AmBe source and comparison to data. For this comparison, the proper ^{124}AmBe nuclear recoil and acceptances were simulated. The simulated events were in agreement with calibration data within statistical uncertainties. Should we show an example, namely a figure from the signal model note?

D. Background Model

The main expected background contribution in the region of interest is due to eviromental and material radioactivity, its composition is mainly represented by Compton scattering photons. Background contribution due to the activation of the xenon 39.6 keV line from radiogenic neutrons is expected to be negligible.

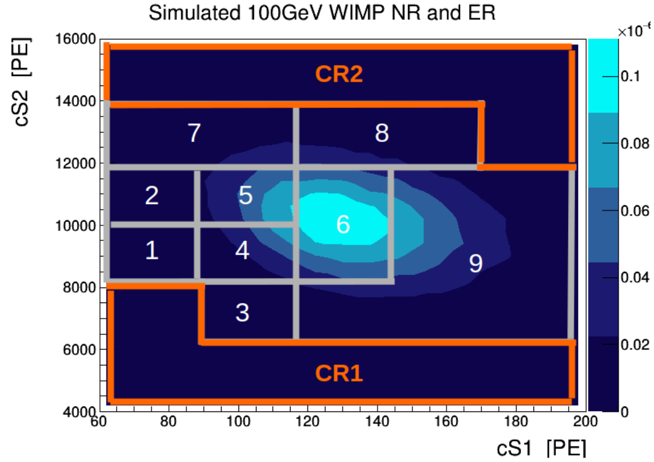

FIG. 2. Simulated signal (1-9) and control (CR1 and CR2) regions for a WIMP mass 100 GeV/c^2.

The background is modeled using data from the ^{60}Co calibration campaign, which are assumed to well represent the background density distribution in the cS1-cS2 plane. The calibration sample yields about 22'000 events in the ROI, these are then scaled to data according to a measured scale factor τ_{bkg}. This scale factor, which is merely the ratio between the data and calibration sample yields, is measured in the two control regions shown in Figure 1 and labelled CR1 and CR2. The two control regions give compatible results and the computed average is $\tau_{bkg} = 0.034 \pm 0.002$, where the reported uncertainty is of statistical nature only.

The distribution of the calibration sample has been compared to the data of the science run in the two control regions, agreement is found within statistical uncertainties. Furthermore, ^{60}Co calibration data have been compared in the region of interest to data from ^{232}Th calibration campaign, the largest deviation between the two shapes is within 4%. An additional systematic uncertainty of 4% has been applied to the expected background yield of each sub-region of the ROI.

E. Systematic Uncertainties

Uncertainties on the total prediction of background events arise from the uncertainty on the measure of the normalization factor, τ_{bkg}, and amount to 6%, contribution of radiogenic neutrons are neglected. Systematic uncertainty on the shape of the predicted background distribution are assessed by the maximal discrepancy in the ROI between the ^{60}Co and ^{232}Th calibration samples, a 4% systematic additional to statistical uncertainty is assigned to the expected yield of each sub-region. Note that uncertainties belonging to different sub-regions are considered independent from each other.

Uncertainty on the total yield of signal arising from selections acceptance uncertainties are found to be very

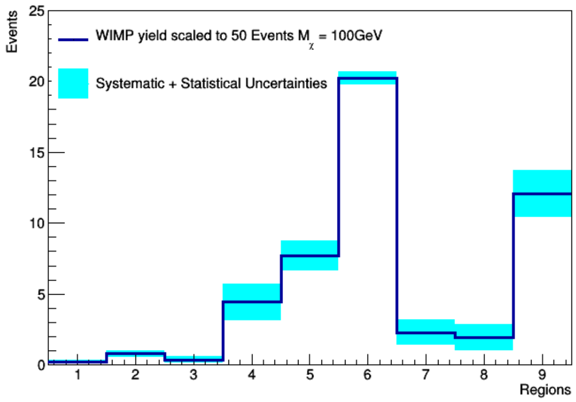

FIG. 3. Signal region, uncertainties for WIMP of mass 100 GeV.

weakly dependent on the WIMP mass, an overall 6% acceptance uncertainty is then applied to all WIMPs hypothesis.

Uncertainties on the energy scale and, more generally, related to detector response are parameterized using the respective uncertainties on the measure of L_y, $\mathcal{L}_{eff}$, Y, Q_Y and ρ. The simulation shows that these type of uncertainties mainly affect the pdf of the signal model in the ROI, and very weakly the total signal yield. They are taken into account by simulating several signal pseudo-sample for each WIMP mass, the pseudo-samples are produced varying the model parameters respectively of ± 1 standard deviation. For each sub-region is then computed an overall uncertainty by adding in quadrature the variations of each pseudo-sample with respect to nominal. Figure 3 is an example of such a systematic uncertainty computation for a WIMP of 100 GeV mass.

All the uncertainties discussed here are parameterized within a binned profiled likelihood function using the framework [24, 25]. All parameters related to systematic uncertainties are assumed to be normally distributed.

IV. RESULTS

Using an exposure of 34 kg of liquid xenon and 224.6 live days of data a yield of 764 events is observed in the region of interest, this is compatible with the expectation of $756 \pm 5^{(stat.)} \pm 55^{(syst.)}$ events from the background only hypothesis. Figure 4 shows how these events are distributed in the region of interest, the bottom panel shows the ratio between data and expected background, where the gray and orange shaded areas represent respectively statistical and systematic uncertainty on the background expectation.

This result is interpreted via a binned profiled likelihood approach by means of the test statistic $\tilde{q}$ and its asymptotic distributions described in [26]. Assuming an isothermal WIMP halo with a local density of $\rho_\chi = 0.3\ GeV/cm^3$, a local circular velocity of $v_0 = 220$ km/s, and a galactic escape velocity of $v_{esc} = 544$ km/s, other assumptions..., a 90% CL$_s$ [27] confidence level limit is computed on the spin dependent inelastic WIMP-nucleon cross section, σ_{inel}, as a function of the WIMP mass, m_χ, and shown in Figure 5. The expected median sensitivity is reported with its relative one (green area) and two (yellow area) standard deviation uncertainty. A limit is set on σ_{inel} to $3.3 \times 10^{-38}\ cm^2$ at 90% CL$_s$ confidence level for a WIMP of mass 100 GeV. This limit is compared with decide which other experiment to plot.

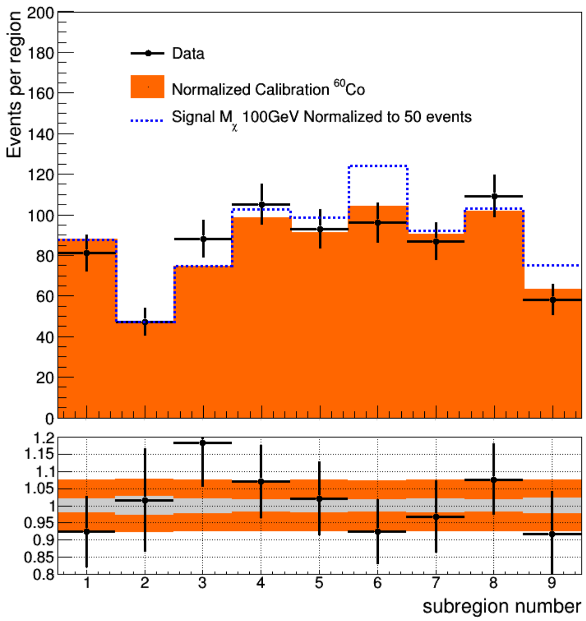

FIG. 4. Results, comparison between data and expected background.

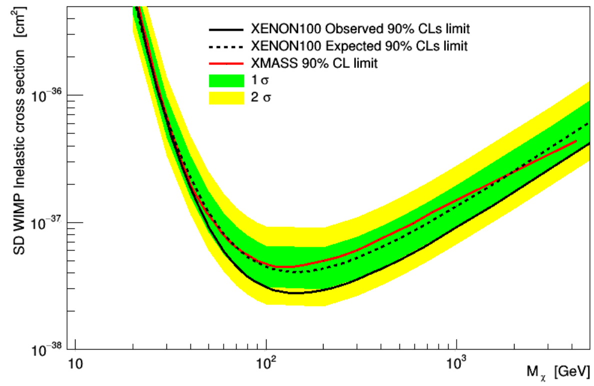

FIG. 5. Observed and expected limits.

[1] J. Silk et al. *Particle Dark Matter: Observations, Models and Searches.* 2010.

[2] Laura Baudis. Dark matter detection. *J. Phys.*, G43(4):044001, 2016.

[3] Laura Baudis. Direct dark matter detection: the next decade. *Phys. Dark Univ.*, 1:94, 2012.

[4] Laura Baudis. Dark matter searches. *Annalen Phys.*, 528:74, 2016.

[5] Teresa Marrodan Undagoitia and Ludwig Rauch. Dark matter direct-detection experiments. *J. Phys.*, G43(1):013001, 2016.

[6] John R. Ellis, R. A. Flores, and J. D. Lewin. Rates for Inelastic Nuclear Excitation by Dark Matter Particles. *Phys. Lett.*, B212:375–380, 1988.

[7] L. Baudis, G. Kessler, P. Klos, R. F. Lang, J. Menendez, S. Reichard, and A. Schwenk. Signatures of Dark Matter Scattering Inelastically Off Nuclei. *Phys. Rev.*, D88(11):115014, 2013.

[8] et al Aprile E. The XENON100 Dark Matter Experiment. *Astropart. Phys.*, 35:573–590, 2012.

[9] E. Aprile et al. Dark Matter Results from 225 Live Days of XENON100 Data. *Phys. Rev. Lett.*, 109:181301, 2012.

[10] E. Aprile et al. XENON100 Dark Matter Results from a Combination of 477 Live Days. *Phys. Rev.*, D94(12):122001, 2016.

[11] E. Aprile et al. Limits on spin-dependent WIMP-nucleon cross sections from 225 live days of XENON100 data. *Phys. Rev. Lett.*, 111(2):021301, 2013.

[12] E. Aprile et al. First Axion Results from the XENON100 Experiment. *Phys. Rev.*, D90:062009, 2014.

[13] E. Aprile et al. Exclusion of Leptophilic Dark Matter Models using XENON100 Electronic Recoil Data. *Science*, 349(6250):851–854, 2015.

[14] E. Aprile et al. Search for Event Rate Modulation in XENON100 Electronic Recoil Data. *Phys. Rev. Lett.*, 115(9):091302, 2015.

[15] E. Aprile et al. Search for Electronic Recoil Event Rate Modulation with 4 Years of XENON100 Data. 2017.

[16] E. Aprile et al. Analysis of the XENON100 Dark Matter Search Data. *Astropart. Phys.*, 54:11–24, 2014.

[17] M Szydagis, A Fyhrie, D Thorngren, and M Tripathi. Enhancement of nest capabilities for simulating low-energy recoils in liquid xenon. *Journal of Instrumentation*, 8(10):C10003, 2013.

[18] John Allison et al. Geant4 developments and applications. *IEEE Trans. Nucl. Sci.*, 53:270, 2006.

[19] S. Agostinelli et al. GEANT4: A Simulation toolkit. *Nucl. Instrum. Meth.*, A506:250–303, 2003.

[20] E Aprile et al. Observation and applications of single-electron charge signals in the xenon100 experiment. *Journal of Physics G: Nuclear and Particle Physics*, 41(3):035201, 2014.

[21] E. Aprile, C. E. Dahl, L. DeViveiros, R. Gaitskell, K. L. Giboni, J. Kwong, P. Majewski, Kaixuan Ni, T. Shutt, and M. Yamashita. Simultaneous measurement of ionization and scintillation from nuclear recoils in liquid xenon as target for a dark matter experiment. *Phys. Rev. Lett.*, 97:081302, 2006.

[22] E. Aprile et al. Dark Matter Results from 100 Live Days of XENON100 Data. *Phys. Rev. Lett.*, 107:131302, 2011.

[23] E. Aprile et al. Response of the XENON100 Dark Matter Detector to Nuclear Recoils. *Phys. Rev.*, D88:012006, 2013.

[24] Lorenzo Moneta, Kevin Belasco, Kyle S. Cranmer, S. Kreiss, Alfio Lazzaro, Danilo Piparo, Gregory Schott, Wouter Verkerke, and Matthias Wolf. The RooStats

Project. *PoS*, ACAT2010:057, 2010.

[25] Wouter Verkerke and David P. Kirkby. The RooFit toolkit for data modeling. *eConf*, C0303241:MOLT007, 2003. [,186(2003)].

[26] Glen Cowan, Kyle Cranmer, Eilam Gross, and Ofer Vitells. Asymptotic formulae for likelihood-based tests of new physics. *Eur. Phys. J.*, C71:1554, 2011. [Erratum: Eur. Phys. J.C73,2501(2013)].

[27] Alexander L. Read. Modified frequentist analysis of search results (The CL(s) method). In *Workshop on confidence limits, CERN, Geneva, Switzerland, 17-18 Jan 2000: Proceedings*, pages 81–101, 2000.